Empirical Mode Decomposition of Pressure Signal for Health Condition Monitoring in Waterjet Cutting

M. Grasso[1], P. Pennacchi, B. M. Colosimo

Dipartimento di Meccanica, Politecnico di Milano, 20133 Milan, Italy

[1] Corresponding author.

Tel.: (+39) 0523-623190

Fax: (+39) 0523-645268

e-mail: marco.grasso@musp.it

***Abstract*— Waterjet/abrasive waterjet cutting is a flexible technology that can be exploited for different operations on a wide range of materials. Due to challenging pressure conditions, cyclic pressure loadings and aggressiveness of abrasives, most of the components of the Ultra High Pressure (UHP) pump and the cutting head are subject to wear and faults that are difficult to predict. Therefore, the continuous monitoring of machine health conditions is of great industrial interest, as it allows implementing condition-based maintenance strategies, and providing an automatic reaction to critical faults, as far as unattended processes are concerned.**

Most of the literature in this frame is focused on indirect workpiece quality monitoring and on fault detection for critical cutting head components (e.g., orifices and mixing tubes). A very limited attention has been devoted to the condition monitoring of critical UHP pump components, including cylinders and valves. The paper investigates the suitability of the water pressure signal as a source of information to detect different kinds of fault that may affect both the cutting head and the UHP pump components. We propose a condition monitoring approach that couples Empirical Mode Decomposition (EMD) with Principal Component Analysis to detect any pattern deviation with respect to a reference model, based on training data. The EMD technique is used to separate high frequency transient patterns from low frequency pressure ripples, and the computation of Combined Mode Functions is applied to cope with the mode mixing effect. Real industrial data, acquired under normal working conditions and in presence of actual faults, are used to demonstrate the performances provided by the proposed approach.

Index Terms — Waterjet Cutting, Condition Monitoring, Empirical Mode Decomposition, Principal Component Analysis

1 INTRODUCTION

Waterjet/abrasive waterjet (WJ/AWJ) machining is a flexible technology that is suitable for different kinds of processes, including cutting, turning, milling and surface treatments, on a wide range of materials [1]. Long duration part-programs are frequently performed in waterjet machining shop floors, leading to a large percentage of unattended processes. In addition, most of the components of the Ultra High Pressure (UHP) pump and the cutting head are subject to wear and faults that are difficult to predict and to avoid. These factors, together with safety requirements and the increasing demand for more effective and efficient

maintenance strategies, i.e. condition-based ones [2], lead to the need for a reliable on-line monitoring and diagnosis equipment.

The need for process monitoring mainly involves the evaluation of the cutting process quality on the one hand, and the health monitoring of critical machine components on the other hand.

Regarding the former issue, problems studied in the literature concern the on-line assessment of cutting stability [3] [4] and the detection of process malfunctions, including non-correct jet penetration [5] [6] and workpiece crack detection when machining brittle materials [7].

With regard to the second stream of research, most of the efforts have been focused on monitoring the conditions of the cutting head components – orifice and mixing tube –, as their health state has a direct impact on the cutting performances (see references from [8] to [13]).

Despite of the actual industrial interest, small attention has been devoted in WJ/AWJ literature to condition monitoring and diagnosis of critical UHP pump components, including cylinders, check valves, seals, etc. (see for example [14] and [15]).

The present study investigates the feasibility of an innovative health monitoring approach based on the analysis of the water pressure signal, aimed at detecting both faults in upstream components (i.e. the UHP pump elements) and in downstream components (i.e. cutting head elements). The pressure signal has the advantage of being easy to acquire in any pump configuration, thanks to the availability of low cost and non-intrusive sensors. The study shows that the pressure signal is multi-scale in nature, and a proper separation of features on different scales may actually improve the detection of critical faults. For such a task, we propose the use of the Empirical Mode Decomposition (EMD), which is a data-driven and adaptive tool that requires neither integral transforms nor basis function definition. The proposed method combines the EMD technique with the Principal Component Analysis (PCA) to summarize the multivariate content of the processed information. The resulting method is called EMD-PCA. The computation of Combined Mode Functions (CMFs) is proposed to cope with the possible mode mixing effect, and to capture the relevant information content of the signal by means of a limited number of modes.

Experimental results based on real industrial data are discussed to show the effects of different faults on the pressure signal pattern. Real data were acquired under normal working conditions and in presence of actual faulty components, and used to test the performances of the proposed approach.

The experimental analysis here presented extends the results discussed by Annoni *et al*. in [11], [12] and [13], by taking into account a larger set of fault conditions and by investigating the multi-scale nature of the pressure signal. The paper also extends the previous work of Colosimo *et al*. [16] on PCA-based process monitoring, by proposing the EMD-PCA technique. The comparison with other PCA-based approaches, and with sample methods commonly used in commercial toolkits adopted in industry, demonstrates the benefits provided by coupling the EMD and the PCA techniques.

To the best of authors' knowledge, condition monitoring based on EMD and PCA, applied to pressure signal, has never been used for WJ/AWJ.

Section 2 briefly introduces the nature of the water pressure signal in WJ/AWJ plants; Section 3 reviews the EMD procedure and the CMF approach; Section 4 presents the proposed EMD-PCA approach; Section 5 describes the experimental setup for real data collection; Section 6 provides a discussion of achieved results; Section 7 eventually concludes the paper.

2 THE PRESSURE SIGNAL IN UHP PUMPS

The most traditional and widespread UHP pump design, involving a water and an oil circuit, is considered in the present study. A pump activated by an electrical motor is used to rise the oil pressure up to a nominal level; the pressurized oil is then sent to the UHP intensifier, which consists of a positive-displacement pump including one or more piston/cylinder groups. The UHP intensifier provides the required water compression to achieve the desired cutting conditions.

Two configurations are mainly adopted for the UHP pump: one based on single-acting plungers, with a single active stroke per cycle, and one based on double-acting plungers, with two active strokes per cycle. The single-acting configuration is considered hereafter.

In case of N parallel single-acting plungers, a complete pumping cycle is composed by N active strokes, shifted in phase. The cycle of each plunger is composed by three distinct steps:

1) the pre-compression step, during which the plunger moves forward, starting from the bottom dead center, and stops when the internal cylinder water pressure equals the water pressure in the discharge circuit;
2) the compression step, which corresponds to the plunger active stroke that pressurizes the water flowing to the cutting head; this step ends at the top dead center;
3) the suction step, during which the water is displaced from the low pressure circuit into the cylinder, until the plunger reaches the bottom dead center, where it is ready for the next cycle.

The entire cycle is regulated by the high pressure (HP) discharge check valves, one for each plunger/cylinder. During the pre-compression step, the HP discharge check valve is closed and the plunger does not actively contributes to the jet; the valve opens only during the compression step, generating the water flow towards the cutting head.

When the water reaches the cutting head and flows through the water orifice, the pressure energy changes into kinetic energy and the jet is formed. If the AWJ is considered, solid particles join the WJ into the mixing chamber, being entrained by the air flow generated by the jet itself. The kinetic energy of abrasive particles is dramatically increased thanks to the momentum exchange with the water inside the mixing chamber and the focusing nozzle.

An example of the pattern of plunger displacement signals and the corresponding pressure signal acquired on the high pressure water line of a three-cylinders pump with single-acting plungers (the same used for the test described in Section 5) is shown in Fig. 1.

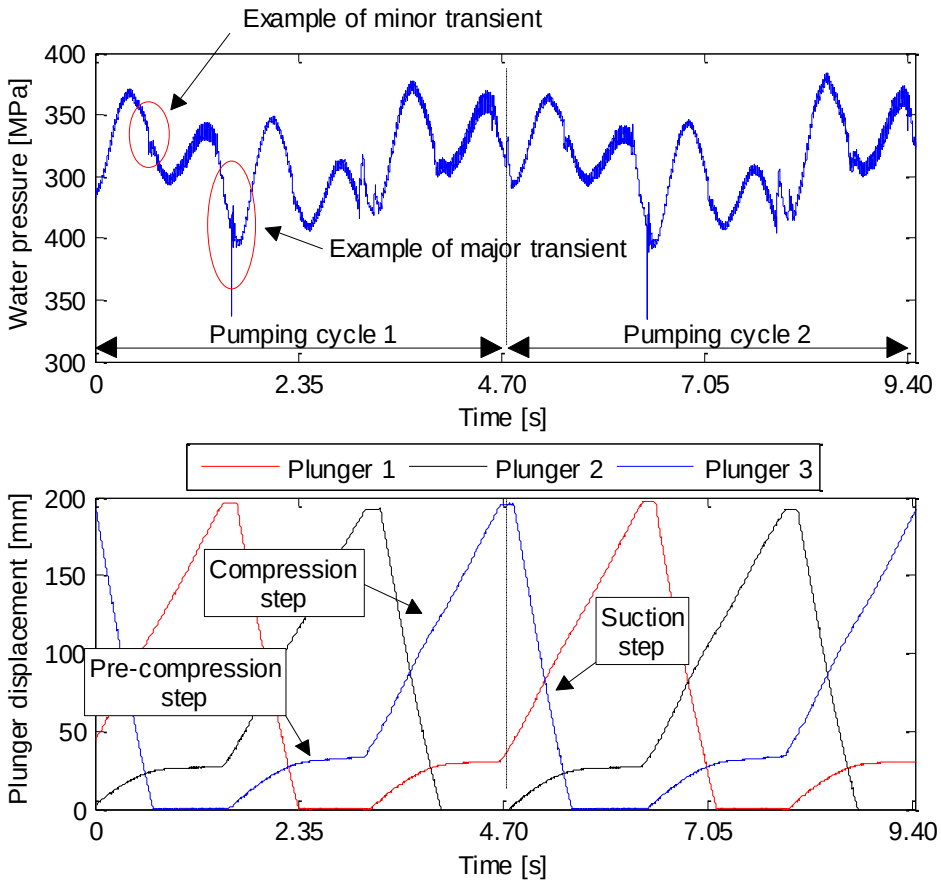

Fig. 1 – Water pressure signal (top) and plunger displacement signals (bottom) for two consecutive pumping cycles

Fig. 1 shows two consecutive pumping cycles. Each cycle is the result of three active strokes shifted in phase. The plunger displacement starts at the bottom dead center (0 mm) and the active stroke ends at the top dead center (about 200 mm). The pressure ripples are due to the plunger kinematics, with major transients corresponding to transitions between the active stroke of a plunger and the active stroke of the next one. When a piston reaches the top dead center, a valve commutation occurs, with a consequent oil flow rate reduction in the next cylinder, resulting in a dynamic pressure discontinuity.

Minor transients are present too, in correspondence of points in time where each plunger completes its suction step. They are caused by a flow rate modification when the piston reaches the bottom dead center.

Both the low frequency and high frequency pressure patterns are difficult to model, since they may be influenced by an instable behavior of the discharge check valves, by water hammer effects in the circuit, etc. For details, see [11] and [15]. Moreover, the water compressibility effect strongly influences the nature of the pumping cycle.

Because of this, the water pressure signal analysis in WJ/AWJ applications is different from traditional fluid power system applications [17] [18] [19].

3 Empirical Mode Decomposition

Conventional methods used for condition monitoring of industrial systems include time-domain analysis of synthetic indexes, power spectrum analysis, cepstrum analysis, etc. One main limitation of those methods consists of the stationarity assumption of the process generating the signals. Time-frequency analysis allows capturing the time-frequency distribution properties of the signal, which often results in an improved extraction of fault features that are localized in time.

Among time-frequency methods used in fault detection and classification applications [20] [21] [22] [23], the wavelet analysis is a very popular approach belonging to the category of linear time-frequency representation techniques. It requires the selection of a proper wavelet basis to match the signal structure, together with a proper choice of decomposition levels and thresholding settings for signal denoising. Ill-selected basis may yield poor results, and the time-frequency resolution may be limited with respect to other methods [24]. To overcome some limitations of the linear time-frequency representation, non-parametric and adaptive methods where proposed by different authors. In this frame, EMD is a powerful method proposed by Huang et al. [25], which allows decomposing any signal into a number of Intrinsic Mode Functions (IMFs). The IMFs represent the natural oscillatory modes embedded in the signal. EMD is completely data-driven and adaptive in nature: it requires neither any integral transform nor the definition of any basis function. IMFs are determined by the signal itself and they work as basis functions. This makes the EMD method a more flexible and efficient tool, which may yield a finer time-frequency resolution than the wavelet transform (for some comparative analysis see [24], [26] and [27]).

Several applications of EMD have been proposed for condition monitoring of gearboxes [28], bearings [29], structural components [30], and also for bio-medical signal monitoring [31] and for power quality assessment [32].

In the frame of fluid power system monitoring applications, EMD was used by Goharrizi *et al.* in [33] where EMD and Hilbert Spectrum are applied for leakage detection in valve-controlled hydraulic actuators.

3.1 The EMD algorithm

The IMFs that capture simple oscillation modes involved in the signal are extracted by means of the *"sifting"* process, which consists of the following steps [25]:

1) All the local minima and maxima of the signal $\mathbf{x} = [x_1,...,x_P]$, where P is the number of time window data points, are identified and they are interpolated respectively by an upper and a lower envelope expressed on a cubic spline basis;
2) The mean of the two envelopes is computed and designated as $\mathbf{m}_1$; then the difference between the signal $\mathbf{x}$ and $\mathbf{m}_1$ is computed and designated as $\mathbf{h}_1$:

$$\mathbf{h}_1 = \mathbf{x} - \mathbf{m}_1 \tag{1}$$

   If $\mathbf{h}_1$ is an IMF, i.e., if $\mathbf{h}_1$ satisfies the following conditions:

   a) in the entire dataset, the number of extremes and the number of zero crossings must be either equal or different at most by one;
   b) at any point, the mean value of the envelope defined by the local maxima and the envelope defined by the local minima is zero;

   then, $\mathbf{h}_1$ is taken as the first IMF of the signal and designated as $\mathbf{c}_1$. If $\mathbf{h}_1$ is not an IMF, $\mathbf{h}_1$ replaces the original signal and the above steps are repeated until an IMF is obtained.
3) The first IMF $\mathbf{c}_1$ is separated from the signal $\mathbf{x}$ by:

$$\mathbf{r}_1 = \mathbf{x} - \mathbf{c}_1 \tag{2}$$

4) The residue $\mathbf{r}_1$ is treated as the original signal and the above steps are repeated, leading to the extraction of following IMFs $\mathbf{c}_1,...,\mathbf{c}_n$, such that:

$$\begin{gathered} \mathbf{r}_1 - \mathbf{c}_2 = \mathbf{r}_2 \\ ... \\ \mathbf{r}_{n-1} - \mathbf{c}_n = \mathbf{r}_n \end{gathered} \tag{3}$$

At the end of the process, the signal is decomposed into n intrinsic modes and a residue $\mathbf{r}_n$:

$$\mathbf{x} = \sum_{i=1}^{n} \mathbf{c}_i + \mathbf{r}_n \tag{4}$$

The residue is a signal such that no further decomposition is possible.

Different stop criteria have been proposed (the interested reader may refer to [34]). In this study, the Amplitude Ratio criterion proposed by Rilling *et al.* [35] is used.

3.2 The Combined Mode Function method

A critical issue is represented by the possible occurrence of the "*mode mixing"* effect [36], when EMD is applied to noisy signals. An intrinsic mode may be split into two or more IMFs in practical applications, and the effect of noise may yield an over-decomposition of the signal, causing the so-called mode mixing. This problem actually limits the reliability of a monitoring scheme that involves the analysis of a single IMF in different time windows. Different approaches have been proposed to cope with such an issue. Huang and Wu [36] proposed a method called Ensemble EMD (EEMD), which consists of defining the true IMF components as the mean of an ensemble of trials, each consisting of the signal plus a white noise of finite amplitude.

A multiscale condition monitoring approach based on EEMD is proposed in [37] and [38]. The main limitation of EEMD is the computational cost, as it requires the computation of a sufficient number of ensemble trials. A computationally efficient variant of EEMD was proposed in [39], but the computational cost is considerably higher than the basic EMD, and this makes EEMD-based monitoring methods poorly attractive as far as on-line applications are concerned.

Intermittency test is another method proposed to face with mode mixing [36]. However, the *a priori* subjective nature of the criterion actually imposes some limits to its practical potential [36].

A more interesting and effective approach for on-line implementation is based on Combined Mode Function (CMF) computation [40].

The CMF approach consists of combining neighboring IMFs $\mathbf{c}_i, \mathbf{c}_{i+1}, ..., \mathbf{c}_{i+q}$ to obtain CMFs as follows:

$$\mathbf{c}_s = \mathbf{c}_i + \mathbf{c}_{i+1} + ... + \mathbf{c}_{i+q} \tag{5}$$

where $1 \le k \le n - q$, being n the maximum number of IMFs. Such a combination of subsets of IMFs can be interpreted as a new adaptive filter bank, which is based on the intrinsic time scales of the signal, resulting in an accuracy increase of the EMD [40].

How to decide which IMFs should be combined together and how to identify subsets of relevant IMFs, actually depends on the specific application. In some applications the goal is to divide the IMFs into two subsets and then to retain just the combination of modes into one of them, either to de-noise or to de-trend the signal [41]. In most diagnostic applications, instead, the need to extract specific fault features focuses the analysis on a limited set of physically relevant IMFs [42] [43]. Thresholding methods based on IMFs' average value [31], IMFs' energy [41], IMFs' correlation with respect to the original signal [44], IMFs' peak frequency [45], and other indexes [28] have been proposed. However, the actual reliability of fully automated selection strategies is still quite doubtful, especially in presence of noisy signals, and context knowledge is often of fundamental importance [44]. The choice is left to the operator in many applications, based on his experience and on the visual analysis of the resulting signal decomposition, under natural process conditions.

In the frame of pressure signal monitoring in WJ/AWJ cutting, modes related to transients should be combined together and separated from those related to low frequency ripples (combined into a different subset) to achieve the highest performances.

4 The proposed approach

The proposed condition monitoring approach combines the computation of CMFs based on EMD, and a PCA-based statistical monitoring approach. The resulting method is called EMD-PCA and it is schematized in Fig.2.

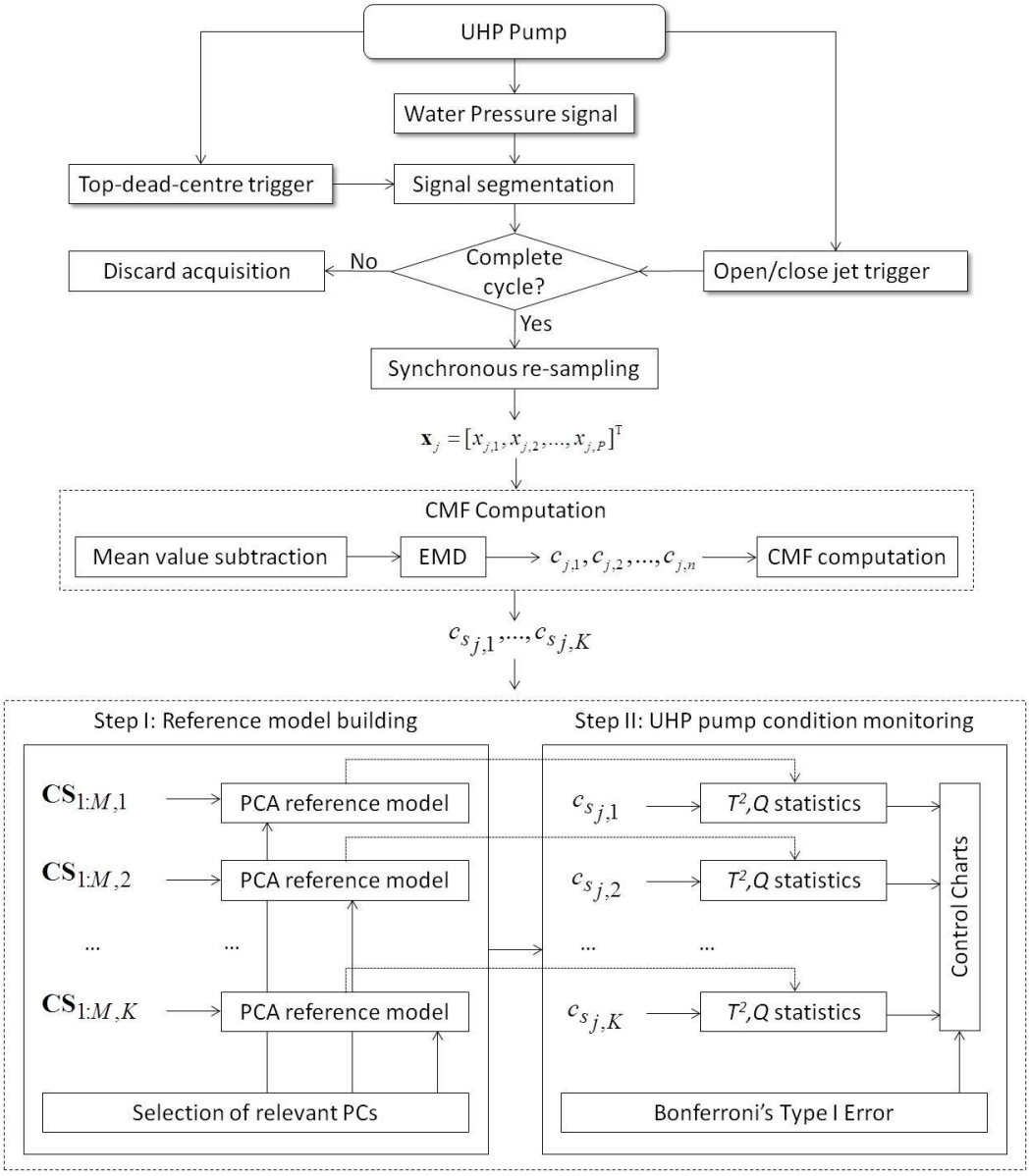

Fig. 2 – Scheme of the proposed condition monitoring approach

The pressure signal is acquired during the cutting process and it is segmented on-line by using the plunger top dead center triggers, normally used by the machine control system. Those triggers allow an automatic segmentation of the signal time series into consecutive time windows. Each window corresponds to a pumping cycle. Furthermore, the acquisition of the open/close jet trigger allows extracting only complete pumping cycles performed without jet interruption. A synchronous re-sampling procedure is then applied to each segment, in order to obtain time windows of constant length. The time reference is converted into a new reference expressed as the percentage of a complete pumping cycle. The new reference step is selected to obtain a window length equal to a power of 2. Then, a periodic cubic

spline interpolation is used to compute the pressure signal values in the new reference points.

Once the synchronous re-sampling step is concluded, the resulting signal is a sequence of observation vectors $\mathbf{x}_j = [x_{j,1}, x_{j,2}, ..., x_{j,P}]^T$, where $j = 1,2,...$ is the index of consecutive time windows, and $P = 2^q$, $q \in \mathrm{N}$, is the fixed number of data points in each time window.

Since the goal consists of analyzing the dynamic pressure fluctuations, the EMD is applied to signal segments $\mathbf{x}_j$ after subtracting the mean value to each segment.

A static pressure monitoring system, i.e. an embedded algorithm devoted to in-process monitoring of the mean pressure level, is already implemented in most WJ/AWJ machine tools. It is designed to terminate the process whenever an unnatural mean pressure drop is observed. However, it is suitable to detect only large leakages, whereas a dynamic pressure analysis method is expected to allow detecting small leakages and incipient faults, in addition to the capability of wear level assessment.

Moreover, the subtraction of the mean pressure level improves the robustness of the monitoring tool, by removing possible misleading effects caused by small static pressure fluctuations associated to the natural variability of the process.

The result is a collection of IMFs $\mathbf{c}_{j,1}, \mathbf{c}_{j,2}, ..., \mathbf{c}_{j,n}$ and a residue signal $\mathbf{r}_{j,n}$ for each complete pumping cycle. Such a signal processing is applied to both the two distinct steps of the monitoring procedure, that are, respectively, the *training step* for reference model building (called step I) and the actual *process monitoring step* (step II).

During step I, a dataset of signals acquired under normal working conditions (reference conditions) is collected. Such a dataset must be representative of the healthy state of the machine tool in the current operative mode, and it will be used as the *reference* for any following fault detection.

The need for a dedicated training step characterizes any data-driven approach. The avoidance of a training step can be achieved only by using model-based methods, but the resulting benefit is counterbalanced by the challenging development of accurate models, and by the need for extended validation experiments. Different authors proposed statistical process monitoring techniques that allow reducing the dependence on large training datasets: they are called *self-starting control charts*

[46]. In principle, they could be coupled with the method here proposed, but the subject goes beyond the scope of the paper.

The step I dataset may be represented in terms of a $M \times P$ matrix $\mathbf{X}$, where M is the number of complete cycles acquired in this step, and each row corresponds to a time window of the original signal:

$$\mathbf{X} = \begin{bmatrix} x_{1,1} & x_{1,2} & \dots & x_{1,P} \\ x_{2,1} & x_{2,2} & \dots & x_{2,P} \\ \dots & \dots & \dots & \dots \\ x_{M,1} & x_{M,2} & \dots & x_{M,P} \end{bmatrix} \tag{6}$$

The EMD is applied to each row of the matrix and IMFs are combined into a number K of CMFs $\mathbf{c}_{s_{j,1}}, \mathbf{c}_{s_{j,2}}, ..., \mathbf{c}_{s_{j,K}}$.

Then, in order to evaluate the stability over time of the CMFs, a PCA-based monitoring scheme is applied [49].

The PCA is a statistical method to explain the variance-covariance structure of a multivariate dataset by means of a few linear combinations of the original variables [47]. Therefore, it is widely used in data analysis and dimensional reduction problems. In the frame of signal processing and process monitoring, the usage of PCA has been proposed and applied by several authors [48] [50] [15]. When the technique is applied to monitor repeating signal profiles over time, as in the present study, the reference procedure is that described by Colosimo *et al.* in [15].

The combination of EMD and PCA has been proposed by some authors to improve signal processing performances of noisy signals with respect to the classical EMD approach [51] [52]. In the present study, the two techniques are combined to develop a multi-scale monitoring tool, where PCA is applied to the CMFs resulting from the EMD of the water pressure signal.

The approach works as follows. Let $\mathbf{c}_{s_{j,k}} = [c_{s_{j,1,k}}, ..., c_{s_{j,P,k}}]^{\mathrm{T}}$ be the k^{th} CMF in j^{th} time window, where $k = 1, \dots, K$, and let $\mathbf{CS}_{1:M,k}$ be a $M \times P$ matrix including the k^{th} CMFs in M pumping cycles collected under normal working conditions (step I):

$$\mathbf{CS}_{1:M,k} = \begin{bmatrix} c_{s1,1,k} & c_{s1,2,k} & \cdots & c_{s1,P,k} \\ c_{s2,1,k} & c_{s2,2,k} & \cdots & c_{s2,P,k} \\ \cdots & \cdots & \cdots & \cdots \\ c_{sM,1,k} & c_{sM,2,k} & \cdots & c_{sM,P,k} \end{bmatrix} \quad (7)$$

The PCA-based monitoring approach then consists of performing a spectral decomposition of the sample correlation matrix $\mathbf{R}_{1:M,k}$ of $\mathbf{CS}_{1:M,k}$, i.e., finding the matrices $\mathbf{L}_k$ and $\mathbf{U}_k$ which satisfy the relationship:

$$\mathbf{U}_k^{\mathrm{T}} \mathbf{R}_{1;M,k} \mathbf{U}_k = \mathbf{L}_k \quad (8)$$

where $\mathbf{L}_k$ is a diagonal matrix whose diagonal elements are the eigenvalues of $\mathbf{R}_{1:M,k}$ ($\lambda_{p,k}$; $p = 1,...,P$), while $\mathbf{U}_k$ is an orthonormal matrix whose p^{th} column $\mathbf{u}_p$ is the p^{th} eigenvector of $\mathbf{R}_{1:M,k}$.

The vector of the j^{th} Principal Component (PC) computed on the K CMFs is defined as follows:

$$\mathbf{z}_{j,k} = \mathbf{U}_k^{\mathrm{T}} \mathbf{c}_{sj,k} = \left[z_{j,1,k},...,z_{j,P,k} \right]^{\mathrm{T}} \quad (9)$$

Then, the process monitoring strategy based on PCA requires the computation of two statistics [15]: one is the Hotelling's T^2 statistics, used to detect possible deviations along the directions of the first m_k PCs (the strategy to select the number m_k is discussed below), for the k^{th} CMF ($k = 1, \ldots, K$):

$$T_{j,k}^2(m_k) = \sum_{l=1}^{m_k} \frac{z_{j,l,k}^2}{\lambda_{l,k}} \quad (10)$$

The second is the Q statistics, used to detect possible deviations in directions orthogonal to the ones associated to the first m_k PCs for the k^{th} CMF ($k = 1, \ldots, K$), given by:

$$Q_{j,k}(m_k) = \left(\mathbf{c}_{s_{j,k}} - \hat{\mathbf{c}}_{s_{j,k}} \right)^{\mathrm{T}} \left(\mathbf{c}_{s_{j,k}} - \hat{\mathbf{c}}_{s_{j,k}} \right) \quad (11)$$

where $\hat{\mathbf{c}}_{s_{j,k}}$ is the reconstruction of CMF $\mathbf{c}_{s_{j,k}}$ after retaining the first m_k PCs, computed as follows:

$$\hat{\mathbf{c}}_{s_{j,k}} = \bar{\mathbf{c}}_{s,k} + \sum_{l=1}^{m_k} z_{j,l,k}\mathbf{u}_p \tag{12}$$

where $\bar{\mathbf{c}}_{s,k}$ is the mean k^{th} CMF among the M observations collected in step I. Obviously, a critical issue is how to select the number m_k of the most important PCs to be retained, for the k^{th} CMF. For a comparative analysis of methods dedicated to such a task see e.g. [53]. Here the number m_k is chosen by applying the Wold's approach [54], which is based on a cross-validation algorithm. At each step of the procedure, one row is deleted from the matrix $\mathbf{CS}_{1:M,k}$ and it is re-estimated by performing the PCA of the remaining rows. The estimation is repeated for increasing values of m_k. For each possible choice of m_k, the Q statistics is computed (eq. (11)). The procedure is repeated for all the rows of the matrix, and the *PRESS* (PRediction Error Sum of Squares) statistics is computed as the grand average of the Q values divided by P:

$$PRESS(m_k) = \frac{1}{MP}\sum_{j=1}^{M} Q_{j,k}(m_k) \tag{13}$$

Eventually the following ratio is computed:

$$R = \frac{PRESS(m_k)}{\sum_{j=1}^{M}\sum_{p=1}^{P}\left(\hat{c}_{s_{j,p,k}}(m_k - 1) - c_{s_{j,p,k}}\right)^2} \tag{14}$$

The R ratio compares the *PRESS* statistics, obtained by retaining m_k PCs, with the sum of squared differences between CMF values $c_{s_{j,p,k}}$ and the CMF values $\hat{c}_{s_{j,p,k}}$, estimated by using all the M rows, but retaining only $m_k - 1$ PCs. Wold showed [54] that, if a ratio $R < 1$ is got, a better prediction is obtained by using m_k instead of $m_k - 1$ PCs. Hence m_k is selected as the highest value such that $R < 1$. For each CMF computed in step II, the T^2 and Q statistics are estimated by using the reference PCA model that includes the matrices $\mathbf{L}_k$ and $\mathbf{U}_k$ and the value of m_k estimated on the step I dataset. Then a control chart is applied to each statistics. The step II control limit used for T^2 control chart is:

$$UCL_{T^2,k} = a_k F_\alpha(m_k, M - m_k) \tag{15}$$

where α is the type I error, whereas $F_\alpha(m_k, M-m_k)$ is the $(1-\alpha)\%$ percentile of the Fisher distribution with m_k and $M-m_k$ degrees of freedom (dofs), respectively, and a_k is given by:

$$a_k = m_k(M+1)(M-1)/M(M-m_k) \tag{16}$$

Regarding the Q statistics, here the control limit formulation proposed by Nomikos and MacGregor [55] is applied: it is computed as follows:

$$UCL_{Q,k} = g_k \chi^2_\alpha(h_k) \tag{17}$$

where $\chi^2_\alpha(h_k)$ is the $(1-\alpha)\%$ percentile of a χ^2 distribution with h_k dofs. The parameters g_k and h_k are estimated as $g_k = \frac{\hat{\sigma}^2_{Qk}}{2\overline{Q}_k}$ and $h_k = \text{int}\left(\frac{2\overline{Q}_k^2}{\hat{\sigma}^2_{Qk}}\right)$, where $\overline{Q}_k$ and $\hat{\sigma}^2_{Qk}$ are respectively the sample mean and sample variance of Q statistics for all the M step I observations, for the k^{th} CMF.

The two control charts refer to two disjoint sets of PCs. Thus, in order to guarantee a type I error (i.e. the expected false alarm rate) equal to the desired one, the Šidák correction for independent events [56] should be used. Given a desired type I error α', then:

$$\alpha = 1-\sqrt{1-\alpha'} \tag{18}$$

The same procedure is repeated for each CMF, i.e. for $k = 1,...,K$, and eventually the Bonferroni's method is adopted to guarantee an overall type I error equal to the selected one, i.e., for a given choice of type I error α', the value used in eq. (18) is $\alpha' = \alpha'/K$.

The proposed approach will signal an alarm when at least one control limit violation will be detected in one control chart applied to the CMFs $\mathbf{c}_{s_{j,1}}, \mathbf{c}_{s_{j,2}}, ..., \mathbf{c}_{s_{j,K}}$, with a globally controlled false alarm rate equal to α'.

5 EXPERIMENTAL SET-UP

An experimental analysis was performed to collect real data both under the natural machine healthy conditions, i.e. the reference condition, and in presence of different types of fault.

The tests were performed on a 45 kW pump with $N = 3$ parallel single-acting plungers and a nominal working point characterized by a water pressure of 350 MPa and a water flow rate of 5 l/min, with a 0.25 mm orifice.

The pressure transducer used in the study is a high pressure transducer suitable for water pressure (Gefran TPH sensor), with a measuring range of 0 to 500 MPa. The pressure transducer is mounted on the high pressure water discharge line as shown in Fig. 3.

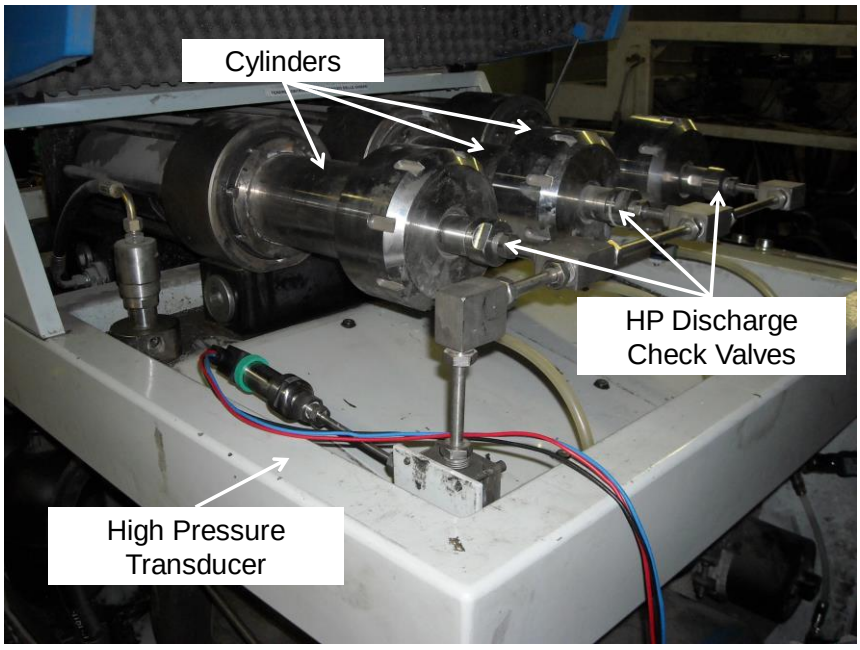

Fig. 3 - Installation of the pressure sensor on the high pressure water discharge line

The faults in the most stressed and critical components have been taken into account. The fault scenarios here considered include:

- a crack in cylinder internal surface - Fault A;
- a crack in HP discharge check valve - Fault B;
- a worn HP discharge check valve seat - Fault C;
- a broken orifice - Fault D.

The former three faults involve critical components of the UHP pump, whereas the last one involves the most critical component of the cutting head, i.e. the orifice. The tests were performed by randomly replicating the execution of the same part-program, consisting of cutting an aluminum laminate, both under normal working conditions and faulty conditions. For details about thetest campaign , see [15] and [57].

Regarding the fault scenarios A, B and C, a different component coming from a real fault was used in each test run and installed into the UHP pump. Regarding Fault D, instead, the effects of a broken orifice were simulated by installing an orifice of the same type, but having a larger diameter (0.33 mm instead of 0.25 mm). An orifice breakage, in fact, usually results in an hole diameter increase, with a consequent pumping frequency increase. Three 0.33 mm orifices were used in fault scenario D.

Faulty components in scenarios A, B and C were ranked in terms of crack severity or wear level. Cracked components were inspected by means of the dye penetrant technique, whereas the worn valve seats were inspected by using a 3D infinite focus microscope. See [15] for details about the nature of faults here considered.

Fig. 4 shows the cracks on internal cylinder surface revealed by dye penetrant technique, and the surface wear of HP discharge check valve seats.

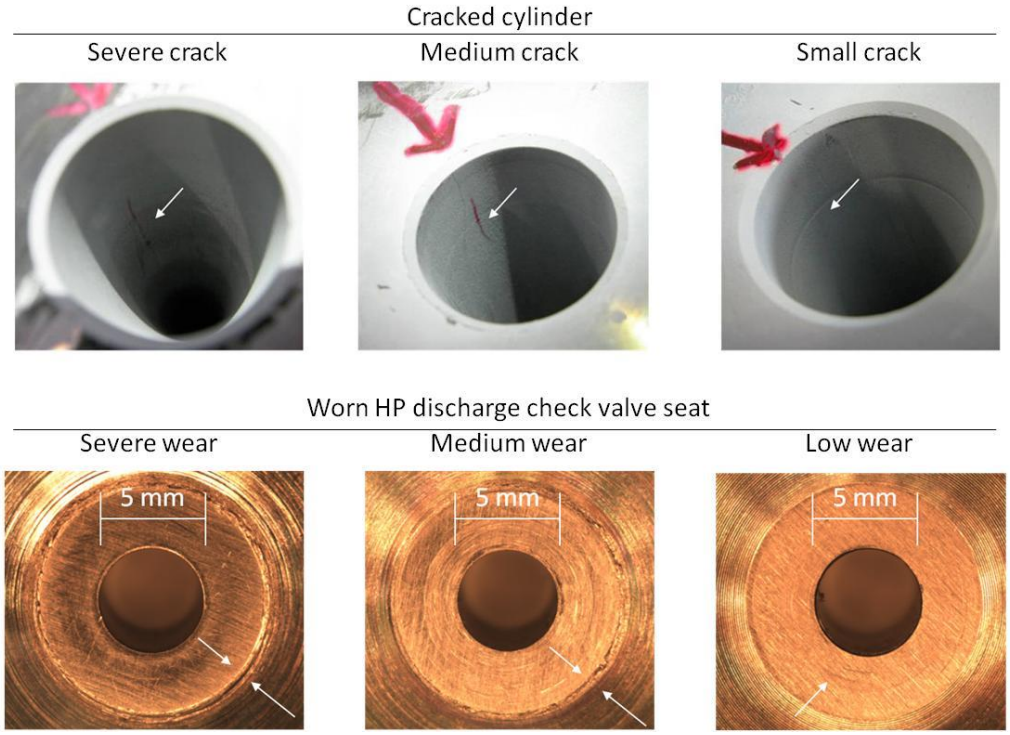

Fig. 4 - Cracks on cylinders revealed by the dye penetrant analysis (top) and damaged surfaces of HP discharge check valve seats (bottom)

A further test run was performed to collect a long pressure signal time series under normal working conditions. In this case, no cut was performed and the signal was acquired with continuously open jet over a time period of about 3 hours. All the other operating conditions were the same discussed above. This additional data acquisition is used to evaluate the performances of the proposed approach in terms of false alarms.

The pumping cycle period under normal working conditions, at the nominal working point of 350 MPa, is about $T = 4.7$ s . The pressure signals were acquired with a sampling frequency of 2 kHz. Such a sampling frequency turned out to be suitable to capture the high frequency transient patterns with sufficient resolution.

6 ANALYSIS OF RESULTS

An example of the decomposition of one complete cycle acquired under normal health conditions is shown in Fig. 5. Regarding the EMD implementation, the Matlab package developed by G. Rilling was used [35].

Fig. 5 shows that the transients between consecutive active strokes are clearly visible in IMF $\mathbf{c}_2$, $\mathbf{c}_3$, and $\mathbf{c}_4$. IMF $\mathbf{c}_1$ captures most of high frequency disturbances and noise, whose amplitude seems to be modulated by the plunger kinematics, with peak-to-peak amplitude increasing as the plunger moves towards the top dead center.

IMF $\mathbf{c}_7$, $\mathbf{c}_8$, and $\mathbf{c}_9$ capture the low frequency pressure ripples, with harmonic content mainly related to multiples of the fundamental frequency $f = 1/T$, up to the 6X harmonic component.

In order to evaluate the goodness of the decomposition, the Orthogonality Index (OI) [25] was computed as follows:

$$OI_j = \sum_{p=1}^{P} \left\{ \sum_{\substack{k=1 \\ q \neq k}}^{n+1} \sum_{q=1}^{n+1} \frac{c_{j,k,p} \cdot c_{j,k,p}}{x_{j,p}^2} \right\} \tag{19}$$

As far as the step I dataset is concerned, the OI sample mean is 0.206 and its sample standard deviation is 0.118.

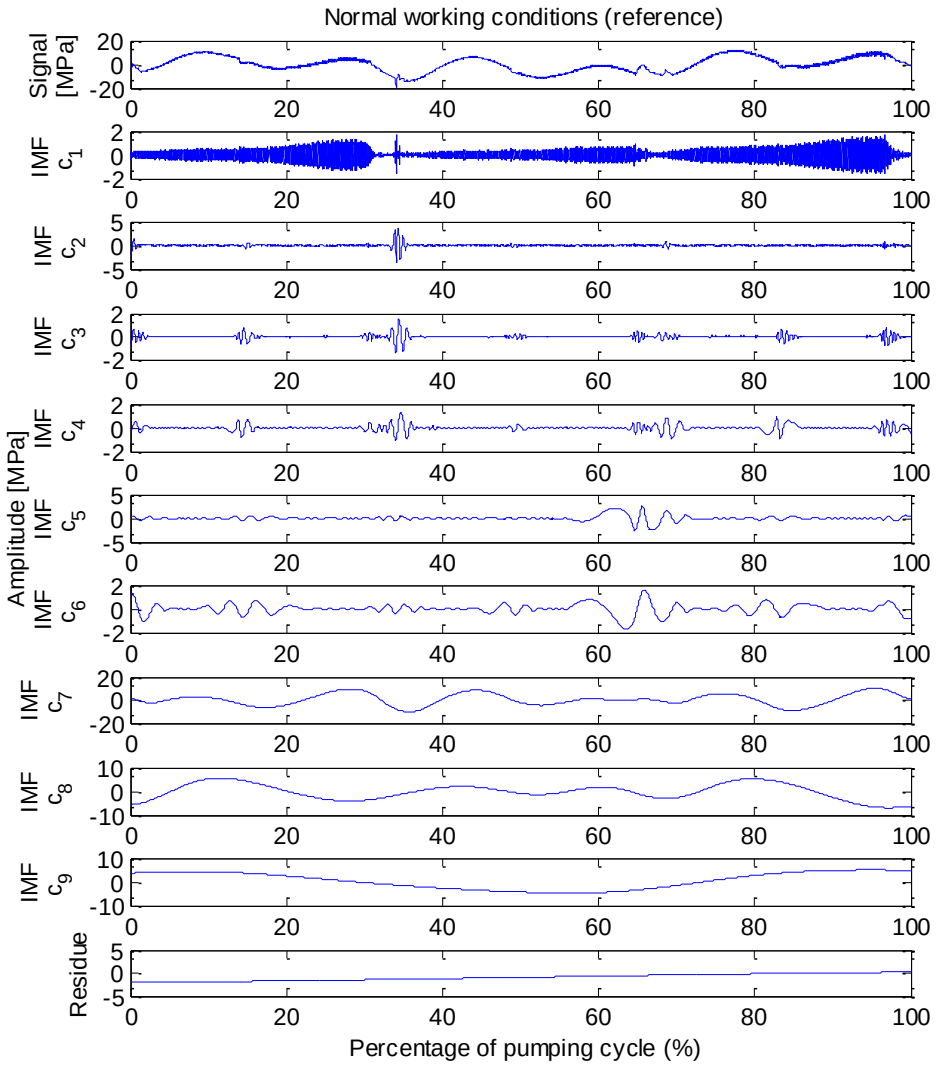

Fig. 5 – EMD of a complete cycle under normal working conditions

The EMDs for each fault scenario are reported in Fig. 6. Fig.6 a) shows the EMD for the cylinder with a large crack in Fault A scenario. Fig. 6 b) shows the EMD for the HP discharge check valve with a medium size crack in Fault B scenario (remember that the run with a severe crack was not performed as the process was stopped by the controller for excessive leakage). Fig. 6 c) shows the EMD for the HP discharge check valve seat with a severe wear level in Fault C scenario. Fig. 6 d) eventually shows the EMD for the broken orifice 1 in Fault D scenario.

As far as Fault A, B and C are concerned, faulty components were installed into the plunger/cylinder group 1.

It is possible to see the evident contraction of the active stroke of plunger 1 when a large crack on the cylinder is present. The effect of the fault affects both the pre-

compression and the compression step of the plunger, with a reduction of the overall single-plunger period. This results in a strong displacement of the transient location, and in a modification of the harmonic content of the signal.

A lower effect is visible in case of Faults B and C. A crack in the HP discharge check valve or a worn valve seat yield a leakage during the pre-compression step only, when the valve is closed. However, the energy of the transients seems to increase with respect to the reference condition, especially in presence of a worn seat.

Fault D, eventually, is a downstream fault and hence it has the same effect on the active strokes of all the plungers. This results in no evident modification of the pumping cycle symmetry, but a slight displacement of transients *a*, *b*, and *c* seems to be presents, probably caused by a different duration of compression and suction steps. A reduction of the 6X harmonic component is a further effect of this fault.

6.1 Selection of the Combined Mode Functions

A critical issue is how to choose the number K of CMFs, and how separate the IMFs into K sub-groups. Since the goal is to separate the modes associated with transient patterns from those associated with low frequency ripples, two groups will be created. In addition, a third group is created by isolating the first IMF $\mathbf{c}_1$, i.e. the one that basically consists of noise and random disturbances, from the remaining IMFs. This allows cleaning the transient modes from noise. The result is the computation of three CMFs, as follows:

$$\mathbf{c}_{s_1} = \mathbf{c}_1 \tag{20}$$

$$\mathbf{c}_{s_2} = \sum_{k=1}^{k_1} \mathbf{c}_k \tag{21}$$

$$\mathbf{c}_{s_3} = \sum_{k=k_1}^{n} \mathbf{c}_k + \mathbf{r}_n \tag{22}$$

where $\mathbf{c}_{s_2}$ should represent the modes associated to transient patterns, and $\mathbf{c}_{s3}$ should represent the modes associated to low frequency ripples.

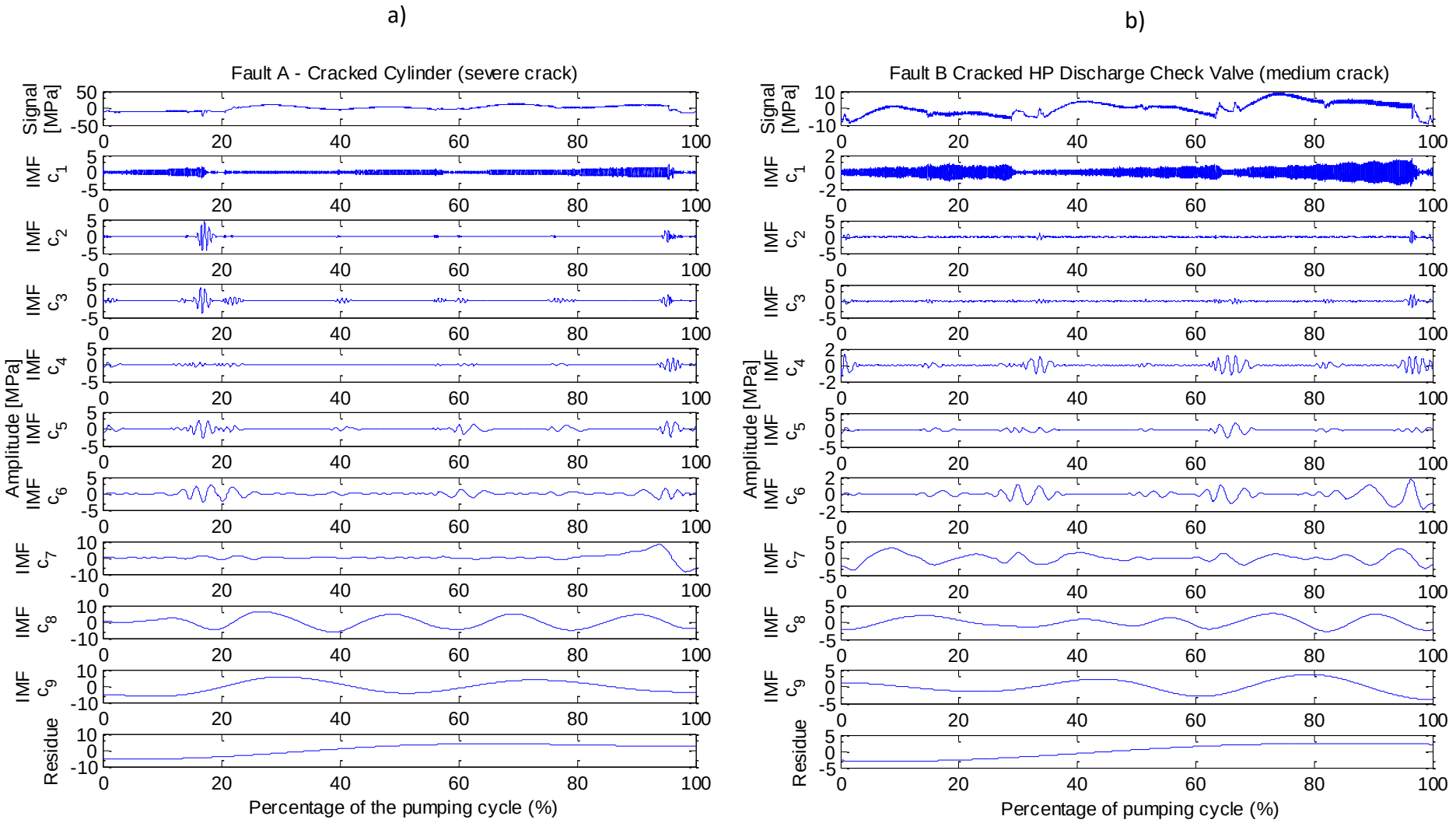

Fig. 6– a) EMD in presence of a severe crack in one cylinder (Fault A), and b) EMD in presence of a medium crack in the HP discharge check valve (Fault B)

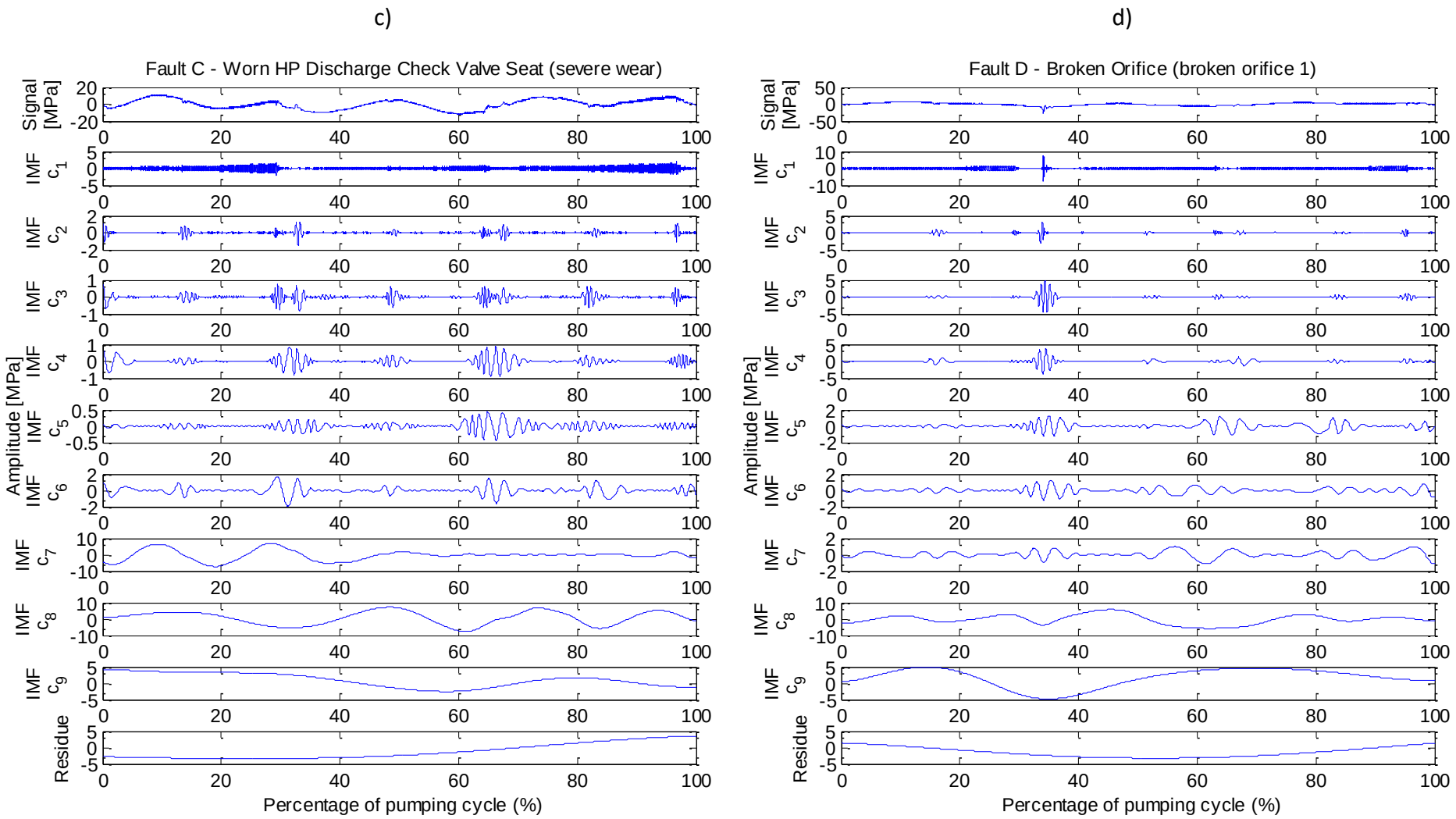

Fig. 6 – c) EMD in presence of a severe wear level of the HP discharge check valve seat (Fault C), and d) EMD in presence of a broken orifice (Fault D)

The residue $\mathbf{r}_n$, which represents the trend term, is included into $\mathbf{c}_{s3}$ since no information content should be lost. Concerning the choice of k_1, i.e. the index of the last IMF included into $\mathbf{c}_{s2}$, two commonly used features are computed: the energy $E_{j,i}$ associated to the i^{th} IMF and the Pearson's correlation coefficient $\rho_{j,i}$ between the i^{th} IMF and the original signal $\mathbf{x}_j$. They are computed respectively as follows:

$$E_{j,i} = \frac{1}{n}\sum_{p=1}^{P} c_{j,i,p}^2 \; ; (i = 1:n) \tag{23}$$

$$\rho_{j,i} = \frac{1}{P} \frac{\sum_{p=1}^{P}\left(c_{j,i,p} - \bar{c}_{j,k}\right)\left(x_{j,p} - \bar{x}_j\right)}{\sqrt{\sum_{p=1}^{P}\left(c_{j,i,p} - \bar{c}_{j,k}\right)^2}\sqrt{\sum_{p=1}^{P}\left(x_{j,p} - \bar{x}_j\right)^2}} \; ; (i = 1:n) \tag{24}$$

Fig. 7 reports the mean values and the standard deviation of the two indexes defined in eq. (23) and eq. (24), i.e., IMF energy and Pearson's correlation between each IMF and the original signal, for the signals acquired under normal working conditions.

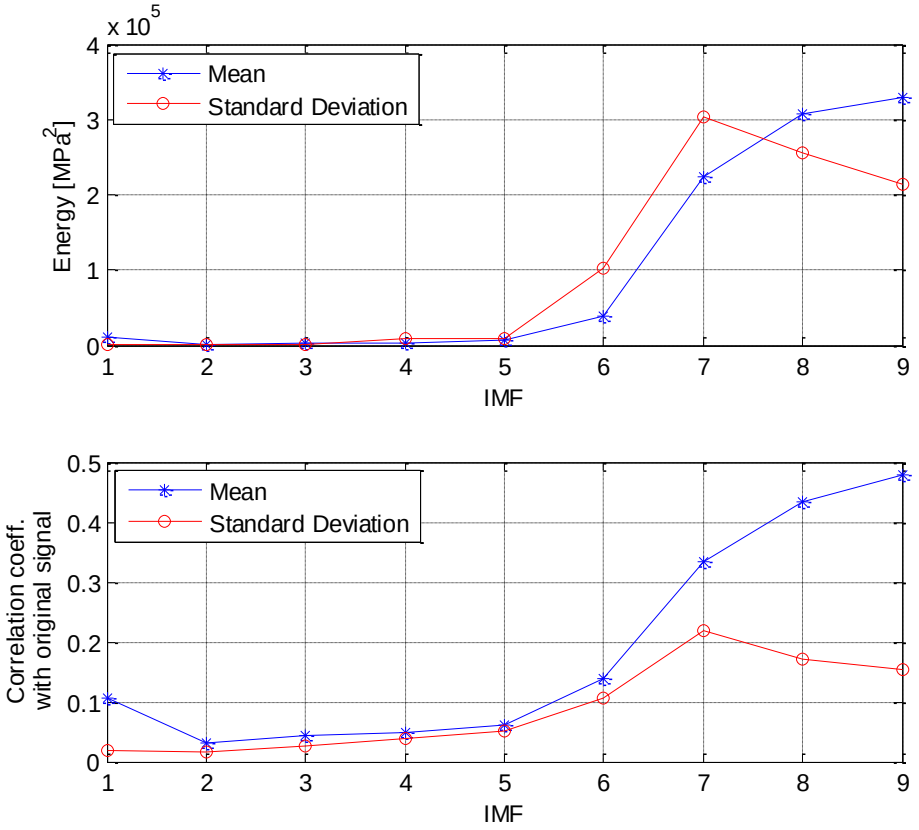

Fig. 7 – Mean value and standard deviation of energy (top) and Pearson's correlation coefficient with respect to original signal (bottom) for each IMF under normal working conditions

Starting from the IMF $\mathbf{c}_6$, there is an evident increase of the mean energy and the energy variability, which also corresponds to an increase of the correlation coefficient.

The observation of Fig. 7 suggests that $k_1 = 6$ (see eq. (21) and eq. (22)) is a bad choice to separate transient modes from low frequency ones. A better choice is represented by $k_1 = 5$. However, by looking at the EMD in Fig. 5, it is evident that the modes that provide the clearest extraction of transient effects are $\mathbf{c}_2$, $\mathbf{c}_3$, and $\mathbf{c}_4$. Thus, a different and maybe more physically consistent choice is represented by $k_1 = 4$.

In order to evaluate the effect of the CMF computation on fault detection performances, three possible solutions are compared, based on the aforementioned choices for the parameter k_1. The resulting monitoring tools are called respectively EMD-PCA 1 ($k_1 = 6$), EMD-PCA 2 ($k_1 = 5$) and EMD-PCA 3 ($k_1 = 4$).

The pattern of $\mathbf{c}_{s_1}$, $\mathbf{c}_{s_2}$ and $\mathbf{c}_{s3}$ with $k_1 = 4$ for the EMD shown in Fig. 5, is reported in Fig. 8, together with the indication of the different steps of the pumping cycle.

The pattern of $\mathbf{c}_{s_2}$ in Fig. 8 clearly captures the transients corresponding to the transitions between different plunger steps. In particular, roman numbers I, II, and III are used to indicate the transients corresponding to the end of active strokes. Transient III is split at the beginning and at the end of the time window, due to the triggering method. Letters *a*, *b*, and *c* are used to indicate transients corresponding to the end of the suction steps. The pattern of $\mathbf{c}_{s_2}$ provides a clear representation of the equal duration of the pumping steps of different plungers.

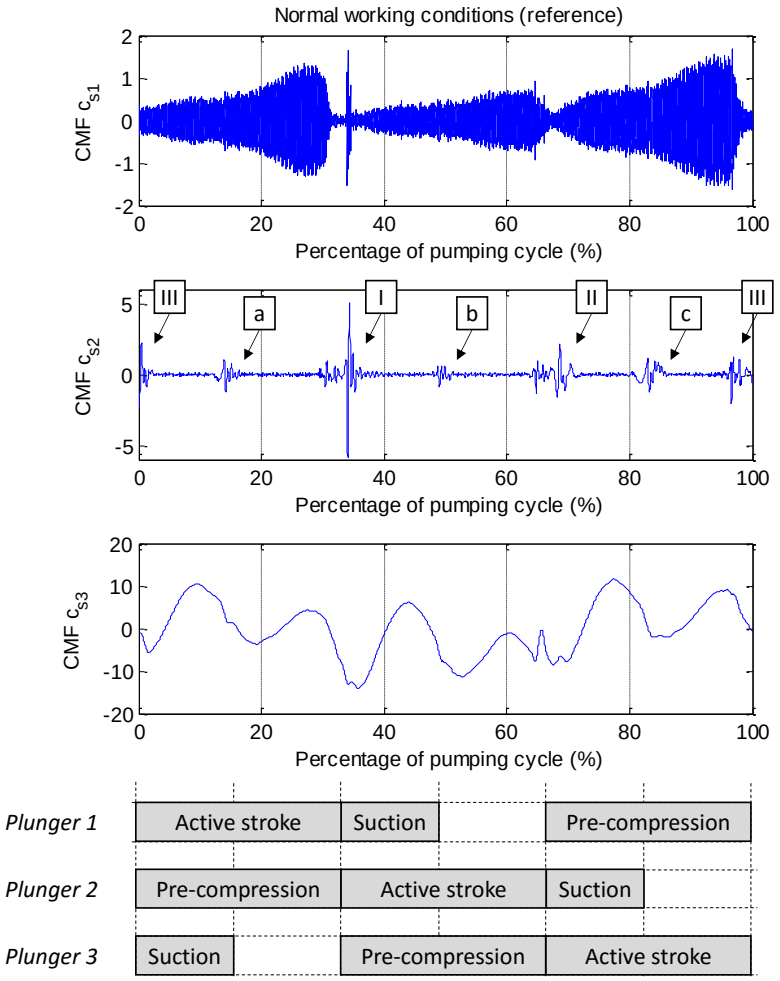

Fig. 8 – Pattern of $\mathbf{c}_{s_1}$, $\mathbf{c}_{s_2}$ and $\mathbf{c}_{s_3}$ with $k_1 = 4$ computed under normal working conditions (top) and indication of the corresponding displacements steps of phased plungers (bottom)

Fig. 9 shows a waterfall plot of the CMF $\mathbf{c}_{s_2}$ with $k_1 = 4$ used in EMD-PCA 3, for both the reference and the faulty signals. In each plot, a set of 10 signals under normal working conditions is shown, followed by sets of the same number of signals acquired under different severity levels in each fault scenario. The waterfall plot clearly shows the modification of transients location caused by Fault A (at least when a large crack is present) and by Fault D (in this case the effect involves only the transients *a*, *b*, and *c*). A transient displacement is visible also in Fault C scenario, when a severely worn seat is installed. Thus, the EMD is expected to extract fault features that are normally hidden by the natural variability of the signals, without concentrating only on low frequency and high amplitude ripples.

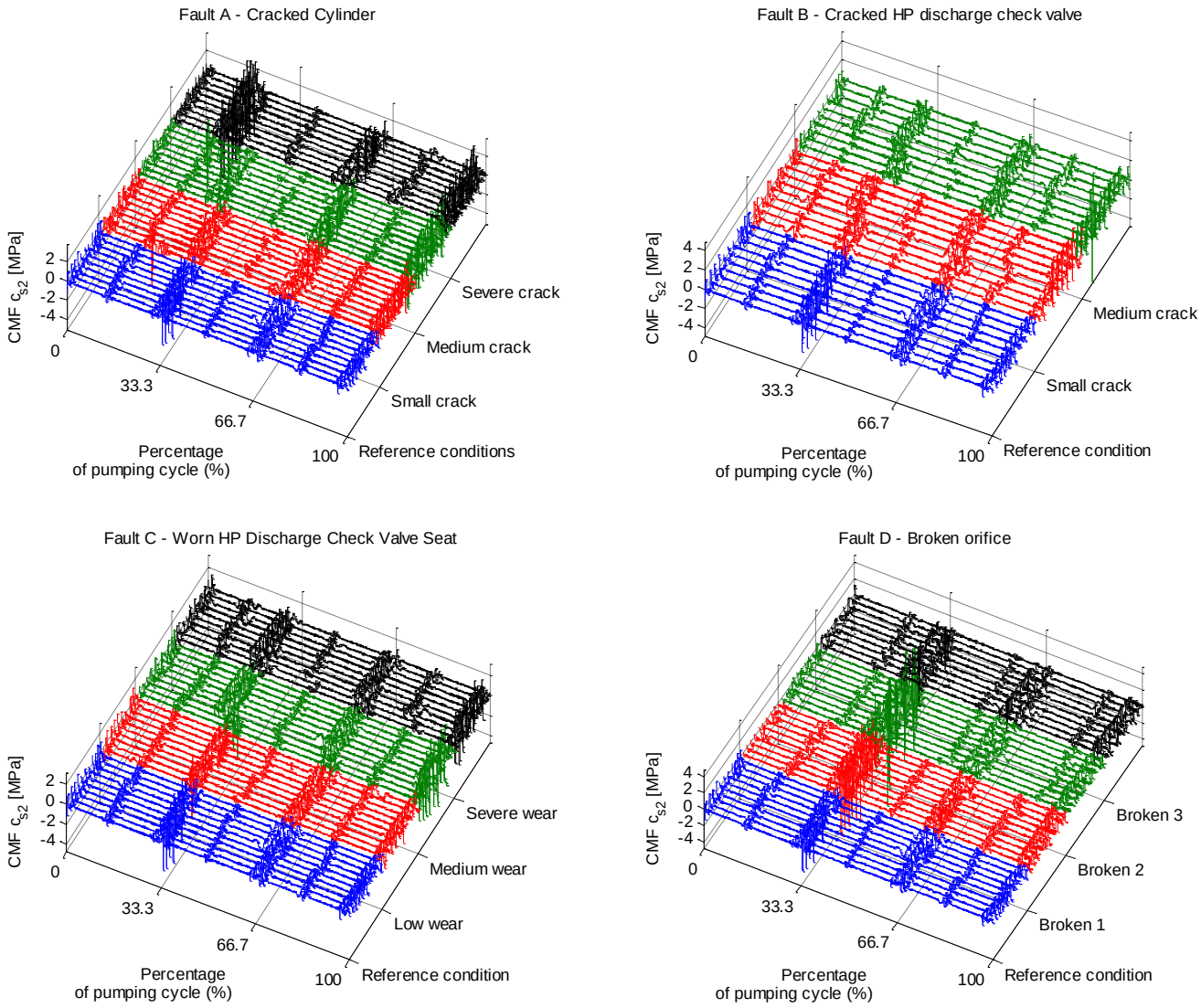

Legend: BLUE: reference condition; RED: small crack (Fault A and B), or low wear (Fault C), or broken orifice 1 (Fault D); GREEN: medium crack (Fault A and B), or medium wear (Fault C), or broken orifice 2 (Fault D); BLACK: severe crack (Fault A), or sever wear (Fault C), or broken orifice 3 (Fault D).

Fig. 9 – Waterfall plot of the CMF $\mathbf{c}_{s_2}$ with $k_1 = 4$ in presence of a) Fault A, b) Fault B, c) Fault C, and d) Fault

6.2 Performance comparison

The EMD-PCA approach was compared with different alternative methods. The goal is to evaluate the possible advantages of the proposed approach over conventional methods commonly used in industry, on the one hand, and with respect to PCA-based methods proposed in literature, on the other hand.

In the frame of industrial approaches, an *index-based* approach and a *Fourier-based* approach were considered. The index-based approach consists of computing time-domain synthetic indexes from the pressure signals. Here the following commonly used indexes are computed: signal standard deviation, skewness, kurtosis, peak-to-peak amplitude and crest factor [17]. The multivariate index vector is monitored by means of a basic T^2 control chart [56]. The Fourier-based method consists of monitoring frequency-domain features: a Fourier-basis expansion is used to estimate the coefficients of relevant harmonics and those coefficients represent the multivariate vector of features to be monitored over time (e.g., see [15]). A basic T^2 control chart is used to monitor the multivariate vector of Fourier coefficients, and a Q control chart is used to monitor the Fourier model residuals. The choice of harmonic components to be included into the model is driven by the power spectrum analysis, possibly supported by goodness-of-fit criteria or other model selection criteria [57]. In this case, the first six harmonic components are included into the model (see Section 2).

In the frame of PCA-based competitor approaches, two methods are considered: the basic PCA-based method proposed by Colosimo and Pacella [16], and a multi-scale PCA approach, which couples the wavelet analysis with the PCA. Different authors proposed different methods to couple the wavelet transform with the PCA (e.g., see [59] [60] [61]). In this study, we consider a common approach, analogous to the one described in [61], which consists of applying the PCA-based control charts to the vector of wavelet coefficients. The wavelet transform based on a 4^{th} order Daubechies mother wavelet is applied to each pressure signal, with a number of decomposition levels selected by using the entropy criterion [62], and the basic PCA approach is applied to the wavelet coefficient vector. No preliminary coefficient selection via thresholding rules is applied. For all the PCA-based methods, the Wold's techniques is used for PCs selection.

All the methods here considered are applied to the signal time windows resulting from the synchronous re-sampling procedure.

The false positive rate performances of the EMD-PCA approach, compared with the Index-based method, the Fourier-based method, the basic PCA-based method and the Wavelet-PCA-based method (here denoted by WPCA), are reported in Table 1, when only signals under normal working condition are monitored.

A type I error value $\alpha' = 0.0027$ is used for all the methods and different sizes of step I dataset are evaluated. The rates reported in Table 1 are based on real data. They refer to the 3 hours-long uninterrupted acquisition, by using the first M pumping cycles as training set.

Table 1 – False positive percentage for the proposed method (EMD-PCA) and the competitor ones

Approach	False positive %		
	$M = 50$	$M = 100$	$M = 150$
Index-based	1.58	2.10	2.44
Fourier-based	1.49	0.71	0.59
PCA	1.49	0.71	0.29
WPCA	1.81	1.07	0.98
EMD-PCA 1	3.77	3.33	3.32
EMD-PCA 2	3.21	1.62	1.51
EMD-PCA 3	0.88	0.81	0.78

The false alarm rate seems to decrease when a larger number of pumping cycles is included into the training dataset, with the only exception of the Index-based approach. The approach that provides the largest percentage of false alarms is the EMD-PCA 1, i.e. the one based on a bad choice of CMF separation.

Such a high percentage may be caused by the possible occurrence of mode mixing effect. A false alarm rate lower than 1% is provided by the Fourier-based, the PCA-based, the WPCA-based and the EMD-PCA 3 approach, when $M = 150$ is used.

A rigorous comparison of actual fault detection performances should be carried out by setting the false alarm rate of all the methods to an equal level. This may be quite troublesome when dealing only with real data and hence such a correction is not applied in the present study. This is expected to introduce only a very limited distortion in the comparative analysis, since the false alarm rates are quite comparable. Furthermore, the methods with the highest false alarm rate, i.e. the Index-based one and the EMD-PCA 1, are also the ones with the lowest fault detection performances.

The results in terms of actual fault detection capability are reported in Table 2. Here the rates correspond to proper alarm signaled when the fault is present. In this case, the complete pumping cycles acquired during the 6 runs of the cutting process under normal working condition have been used ($M = 131$).

Table 2 – Fault detection percentage for the proposed approach (EMD-PCA) and the competitor ones

		Fault Detection %						
		Approach						
Fault	Fault severity	Index based	Fourier based	PCA	WPCA	EMD-PCA1	EMD-PCA2	EMD-PCA3
A	Severe crack	89.3	**100**	**100**	**100**	**100**	**100**	**100**
	Medium crack	67.9	**100**	**100**	**100**	**100**	**100**	**100**
	Small crack	20.0	**100**	**100**	96.0	**100**	**100**	**100**
B	Medium crack	25.9	85.2	**100**	**100**	88.9	**100**	**100**
	Small crack	4.2	95.8	91.7	**100**	79.3	95.8	**96.3**
C	Severe wear	8.3	**100**	**100**	**100**	91.7	**100**	**100**
	Medium wear	19.2	61.5	92.3	96.2	65.4	**100**	**100**
	Low wear	0.0	7.7	57.7	4.2	26.9	**100**	**100**
D	Broken 1	97.1	41.2	47.1	**100**	82.4	**100**	**100**
	Broken 2	5.7	97.1	97.1	**100**	85.7	**100**	**100**
	Broken 3	39.8	88.6	**100**	**100**	32.3	**100**	**100**
	Tot	39.8	81.3	91.6	91.7	77.3	99.2	**99.7**

Table 2 shows that the approach based on time-domain synthetic indexes gives a very poor detection capability. The Fourier-based approach performs better and it allows detecting Fault A at 100% rate. However, the global detection rate is about 81%. The basic PCA-based and the WPCA-based methods provide similar results, with a global detection rate of 91.6 - 91.7%. However, the PCA-based approach yields quite low detection percentages in case of a low wear level in Fault C scenario and for broken orifice 1, whereas the WPCA-based approach yields a very low detection rate for the low wear level in Fault C scenario.

The highest performances are achieved with the EMD-PCA 2 and EMD-PCA 3 approaches, i.e., when a proper choice of CMF separation is adopted. In particular, both the EMD-PCA approaches provide a 100% detection rate for Fault A, Fault C and Fault D, with a slightly missed detection percentage only for the small crack of the HP discharge check valve. However, remember that the EMD-PCA 2 also provides a slightly higher percentage of false alarms than the EMD-PCA 3 and the traditional PCA-based approach.

Table 3 – Fault detection performances for each CMF when the proposed approach (EMD-PCA) is applied, with a) $k_1 = 6$), b) $k_1 = 5$, and c) $k_1 = 4$

		a) Fault Detection % with EMD-PCA 1		
Fault	Fault severity	CMF		
		$\mathbf{c}_{s_1}$	$\mathbf{c}_{s_2}$	$\mathbf{c}_{s_3}$
A	Severe crack	**100**	3.6	**100**
	Medium crack	14.3	0.0	**100**
	Small crack	4.0	0.0	**100**
B	Medium crack	0.0	25.0	**81.5**
	Small crack	37.5	11.1	**50.0**
C	Severe wear	0.0	0.0	**91.7**
	Medium wear	42.3	3.9	**50.0**
	Low wear	7.7	3.9	**23.1**
D	Broken 1	**82,3**	5.9	29.4
	Broken 2	**82.9**	0.0	77.1
	Broken 3	**22.6**	0.0	16.1
		b) Fault Detection % with EMD-PCA 2		
Fault	Fault severity	CMF		
		$\mathbf{c}_{s_1}$	$\mathbf{c}_{s_2}$	$\mathbf{c}_{s_3}$
A	Severe crack	**100**	**100**	**100**
	Medium crack	14.3	42.9	**100**
	Small crack	4.0	16.0	**100**
B	Medium crack	0.0	22.2	**100**
	Small crack	37.5	16.7	**95.6**
C	Severe wear	0.0	8.3	**100**
	Medium wear	42.3	11.5	**100**
	Low wear	7.7	3.9	**100**
D	Broken 1	82,3	5.9	**94.1**
	Broken 2	82.9	42.9	**100**
	Broken 3	22.6	64.5	**100**
		c) Fault Detection % with EMD-PCA 3		
Fault	Fault severity	CMF		
		$\mathbf{c}_{s_1}$	$\mathbf{c}_{s_2}$	$\mathbf{c}_{s_3}$
A	Severe crack	**100**	**100**	**100**
	Medium crack	14.3	**100**	**100**
	Small crack	4.0	52.0	**100**
B	Medium crack	0.0	81.5	**100**
	Small crack	37.5	66.7	**96.3**
C	Severe wear	0.0	88.5	**100**
	Medium wear	42.3	88.5	**100**
	Low wear	7.7	20.8	**100**
D	Broken 1	82,3	**100**	**100**
	Broken 2	82.9	**100**	**100**
	Broken 3	22.6	**100**	**100**

The lower performances provided by the EMD-PCA 1 approach are due to the bad choice of the CFM separation: this demonstrates the importance of a reliable IMF separation criterion.

The detail of fault detection performances for each CMF can be evaluated by looking at Table 3. Table 3 a), b) and c) report, respectively, the fault detection percentages achieved with approaches EMD-PCA 1, EMD-PCA 2 and EMD-PCA 3 for each computed CMF. When EMD-PCA 1 is applied, the fault detection capability of the CMF $\mathbf{c}_{s_1}$ is quite low, and also the fault detection capability of the CMF $\mathbf{c}_{s_3}$ is strongly reduced in case of Fault D.

By using a better definition of CMFs, i.e. in case of EMD-PCA 2 and EMD-PCA 3, the detection capability of both the CMF $\mathbf{c}_{s_2}$ and the CMF $\mathbf{c}_{s_3}$ is considerably improved. In particular the highest contribution of the CMF $\mathbf{c}_{s_2}$ is achieved when only the IMFs $\mathbf{c}_2$, $\mathbf{c}_3$, and $\mathbf{c}_4$ are combined together (EMD-PCA 3).

Table 3 shows that a large crack of the cylinder and a broken orifice have a quite evident effect also on the first IMF, i.e. the one which captures most of the signal noise.

7 CONCLUSIONS

The paper presents a novel approach for health condition monitoring of both the UHP pump and the cutting head components based on the water pressure signal.

In WJ/AWJ applications, different types of fault have different effects on the water pressure signal pattern, as they involve the different steps of the pumping cycle. However, the natural variability of the pressure ripples under normal working conditions may reduce the capability of extracting the relevant fault features. The use of simple time-domain synthetic indices provide very poor fault detection performances. A monitoring approach based on the coefficients of the main harmonic components led to quite better results in the tests here reported, but it filters out intermittent transient patterns, reducing the amount of relevant information.

In order to improve the fault detection performances, we propose the use of EMD as a non-parametric tool for multi-scale decomposition of the pressure signal. The goal consists of isolating the high frequency transient patterns, corresponding to sudden flow rate modifications caused by the displacement steps of phased plungers, from the low frequency pressure ripples. The EMD allows decomposing

the signal by means of a completely data-driven and adaptive algorithm, which requires neither any integral transform nor the definition of any basis function.

The separation of low frequency ripples from intermittent patterns allows capturing pressure signal features at different scales, leading to a better characterization of the effects of different kinds of fault. By using the CMF method, it is possible to cope with the mode mixing effect that may occur during the sifting process, and, at the same time, to synthetize the relevant information content into a small number of modes. The proposed health condition monitoring approach involves a preliminary signal processing step based on the CMFs extraction, followed by the use of PCA-based control charts. The resulting method is a multi-scale extension of previously proposed PCA-based control charts for cyclically repeating waveform signals. The non-parametric and adaptive nature of the EMD technique, together with its fine time-frequency resolution, gives interesting advantages over more commonly used multi-scale methods. The comparative study shows that the EMD-PCA approach may produce a fault detection improvement with respect to basic PCA-based and Wavelet-PCA based approaches. Nevertheless, an exhaustive comparative analysis including different implementations of time-frequency techniques requires further research efforts, possibly supported by extended Monte Carlo simulations.

The main limitation of the EMD consists of the non-orthogonality of the empirical basis, which results in the possible occurrence of the mode mixing effect. The use of CMFs allows coping with such an effect, but the result actually depends on the adopted strategy to separate the IMFs into a reduced number of CMFs. The study highlights the importance of a reliable IMF separation criterion. Different indexes and empirical rules were proposed in literature for such a task, but a decision making process that involves the experience of the operator and the visual analysis of the signal decomposition is still expected to strongly improve the results.

Further research streams may be aimed at developing and testing IMF selection and/or separation criteria to enhance the actual industrial implementability of EMD-based health monitoring tools.

Nomenclature

a	Parameter used in UCL_{T^2} computation
$\mathbf{c}$	Intrinsic Mode Function (IMF)
$\mathbf{c}_s$	Combined Mode Function (CMF)
$\hat{\mathbf{c}}_s$	CMF reconstruction based on reference PCA model
CMF	Combined mode function
$\mathbf{CS}_{1:M}$	Data matrix of CMFs computed from EMD applied on $\mathbf{X}$
EEMD	Ensemble EMD
EMD	Empirical mode decomposition
$F_\alpha(\cdot,\cdot)$	$(1-\alpha)\%$ percentile of the F distribution
g,h	Parameters used for UCL_Q computation
$\mathbf{h}_1$	Difference between signal and envelope mean at sifting step 1
HP	High pressure
IMF	Intrinsic mode function
K	Number of CMFs
$\mathbf{L}$	Diagonal eigenvalue matrix
M	Number of pumping cycles acquired in step I
m	Number of retained PCs
$\mathbf{m}_1$	Envelope mean computed at first sifting process step 1
n	Maximum number of IMFs
N	Number of phased plungers
OI	Orthogonality index
P	Number of data points within each pumping cycle time window
PCA	Principal component analysis
$PRESS$	Prediction Error Sum of Squares
Q	Squared prediction error statistics
R	Wold's statistics for the selection of relevant PCs
$\mathbf{R}_{1:M}$	Correlation matrix of $\mathbf{CS}_{1:M}$
$\mathbf{r}_n$	EMD residual at the end of sifting process
T^2	Hotelling's statistics
$\mathbf{U}$	Eigenvector matrix

UCL_{T^2}	Control limit for the T^2 control chart
UCL_Q	Control limit for the Q control chart
UHP	Ultra high pressure
$\mathbf{x}$	Signal associated to each pumping cycle time window
$\mathbf{X}$	Data matrix used in reference model building step (step I)
WJ/AWJ	Waterjet/abrasive waterjet
$\mathbf{z}$	Principal Component (PC)
α, α'	Type I error
λ	Eigenvalue
$\chi^2_\alpha(\cdot)$	$(1-\alpha)\%$ percentile of the χ^2 distribution

Subscripts

i	IMF index ($i = 1,..., n$)
j	Pumping cycle index ($j = 1,2,...,$)
k	CMF index ($k = 1,..., K$)
l	Principal Component index ($l = 1,..., m_k$)
p	Data point index ($p = 1,..., P$)

Acknowledgments

The authors want to thank Altag Srl and CMS Tecnocut for providing machine availability, resources and materials that made possible the execution of the experimental activity. A special thanks also to Massimiliano Annoni and Massimo Goletti for their fundamental technical support.

References

[1] R. Kovacevic, M. Hashish, R. Mohan, M. Ramulu, T.J. Kim, E.S. Geskin, State Of The Art Of Research And Development In Abrasive Waterjet Machining, Journal of Manufacturing Science and Engineering, Vol. 119, no. 4, pp. 776 – 785, 1997

[2] H. M. Hashemian, State-of-the-Art Predictive Maintenance Techniques, IEEE Transactions on Instrumentation and Measurement, Vol. 60, no. 1, pp. 226 – 236, 2011

[3] V. Perzel, P. Hreha, S. Hloch, H. Tozan, J. Valicek, Vibration Emission As A Potential Source Of Information For Abrasive Waterjet Quality Process Control, The International Journal of Advanced Manufacturing Technology, Vol. 61, no. 1-4, pp. 285 – 294, 2012

[4] T. Krenicky, R. Miroslav, Monitoring Of Vibrations In The Technology Of AWJ, Key Engineering Materials, Vol. 96, pp. 229 – 234, 2012

[5] D. A. Axinte, M. C. Kong, An Integrated Monitoring Method to Supervise Waterjet Machining, CIRP Annals – Manufacturing Technology, Vol. 58, pp. 303-306, 2009

[6] A. Rabani, I. Marinescu, D. Axinte, Acoustic Emission Energy Transfer Rate: A Method For Monitoring Abrasive Waterjet Milling, International Journal of Machine Tools & Manufacture, Vol. 61, pp. 80 – 89, 2012

[7] G.S. Choi, G.H. Choi, Process Analysis And Monitoring In Abrasive Waterjet Machining Of Alumina Ceramics, International Journal of Machine Tools and Manufacture Vol. 37, no. 3, pp. 295-307, 1997

[8] W. Wang, M. Wang, Abrasive Waterjet Process Control Overview, 2011 International Conference on Consumer Electronics, Communications and Networks (CECNet), April 16-18, 2011, Xianning, China

[9] R. S. Mohan, Real-Time Monitoring Of AWJ Nozzle Wear Using Artificial Neural Network, Transactions of the North American Manufacturing Research Institute of SME 1994, Vol. 22, May 25-27, 1994, Evanston, IL, USA

[10] B. Jurisevic, D.Brissaud, M. Junkar, Monitoring Of Abrasive Water Jet (AWJ) Cutting Using Sound Detection, International Journal of Advanced Manufacturing Technology, Vol. 24, pp. 733 – 737, 2004

[11] M. Annoni, L. Cristaldi, M. Lazzaroni, Measurements, Analysis And Interpretation Of The Signals From A High-Pressure Waterjet Pump, IEEE Transactions on Instrumentation and Measurement, Vol. 57, no. 1, pp. 34-47, 2008

[12] M. Annoni, L. Cristaldi, M. Lazzaroni, S. Ferrari, Nozzles Classification in a High-Pressure Water Jet System, IEEE Transactions on Instrumentation and Measurement, Vol. 58, no. 10, pp. 3739 – 3745, 2009

[13] M. Annoni, L. Cristaldi, M. Faifer, Electric Signature Analysis for High Pressure Waterjet Pumps Fault Classification, 16th IMEKO TC4 Symposium – Exploring New Frontiers of Instrumentation and Methods for Electrical and Electronic Measurements, Sept. 22-24, 2008, Florence, Italy

[14] W. Xia, D. Zhao, J. Guo, B. Chen, Research On The Abrasive Water-Jet Cutting Machine Information Fusion Fault Diagnosis System Based On Fuzzy Neural Network, International Conference on Biomedical Engineering and Computer Science (ICBECS), April 23-25, 2010, Wuhan, China

[15] M. Grasso, M. Goletti, M. Annoni, B. M. Colosimo, A New Approach for Online Health Assessment of Abrasive Waterjet Systems, International Journal of Abrasive Technology, Vol. 6, no. 2, pp. 158-181, 2013

[16] B.M. Colosimo, M. Pacella, On the Use of Principal Component Analysis to Identify Systematic Patterns in Roundness Profiles, Quality and Reliability Engineering International, Vol. 23, no. 6, pp. 707-725, 2007

[17] B. K. N. Rao, Handbook of Condition Monitoring, Elsevier Science Ltd, 1996

[18] R.S. Beebe, Predictive Maintenance of Pumps Using Condition Monitoring, Elsevier Science & Technology Books, 2004

[19] Y. Gao, Q. Zhang, X. Kong, Wavelet-Based Pressure Analysis for Hydraulic Pump Health Diagnosis, Transactions of the ASAE – American Society of Agricultural Engineers, Vol. 46, no. 4, pp. 969-976, 2003

[20] T. Kaewkongka, Y. H. J. Au, R. T. Rakowski, B. E. Jones, A Comparative Study of Short Time Fourier Transform and Continuous Wavelet Transform for Bearing Condition Monitoring, International Journal of COMADEM, Vol. 6, no. 1, pp. 41–48, 2003

[21] Z.K. Peng, F.L. Chu, Application of the Wavelet Transform in Machine Condition Monitoring and Fault Diagnostics: a Review with Bibliography, Mechanical Systems and Signal Processing, Vol. 18, no. 2, pp. 199-221, 2004

[22] H. Li, H. Zheng, L. Tang, Wigner-Ville Distribution Based on EMD for Faults Diagnosis of Bearings, Fuzzy Systems and Knowledge Discover, Lecture Notes in Computer Sciences, Vol. 4223, pp. 803-812, 2006

[23] R. Kothamasu, S.H. Huang, W.H. VerDuin, System Health Monitoring and Prognostics – a Review of Current Paradigms and Practices, International Journal of Advanced Manufacturing Technology, Vol. 28, pp. 1012-1024, 2006

[24] Z. Feng, M. Liang, F. Chu, Recent Advances in Time-Frequency Analysis Methods for Machinery Fault Diagnosis: A Review with Application Examples, Mechanical Systems and Signal Processing, Vol. 38, pp. 165-205, 2013

[25] N.E. Huang, Z. Shen, S.R. Long, M.L. Wu, H.H. Shih, et al., The Empirical Mode Decomposition and Hilbert Spectrum for Nonlinear And Nonstationary Time Series Analysis, Proc. R. Soc. London Ser. A, Vol. 454, pp. 903–95, 1998

[26] P. Flandrin, G. Rilling, and P. Goncalves, Empirical mode decomposition as a filter bank, IEEE Sig. Process. Lett, Vol. 11, no. 2, pp. 112–114, 2004

[27] Z.K. Peng, P. W. Tse, F.L. Chu, A Comparison Study of Improved Hilbert-Huang Transform and Wavelet Transform: Application to Fault Diagnosis for Rolling Bearing, Mechanical Systems and Signal Processing, Vol. 19, pp. 974-988, 2005

[28] R. Ricci, P. Pennacchi, Diagnostics of Gear Faults Based on EMD and Automatic Selection of Intrinsic Mode Functions, Mechanical Systems and Signal Processing, Vol. 25, no. 3, pp. 821-838, 2011

[29] D. Yu, J. Cheng, Y. Yang, Application of EMD method and Hilbert Spectrum to the Fault Diagnosis of Roller Bearings, Mechanical Systems and Signal Processing, Vol. 19, pp. 259-270, 2005

[30] D. Pines, L. Salvino, Structural Health Monitoring using Empirical Mode Decomposition and the Hilbert Phase, Journal of Sound and Vibration, Vol. 294, pp. 97-124, 2006

[31] H. Liang, Q-H. Lin, J.D.Z. Chen, Application of the Empirical Mode Decomposition to the Analysis of the Esophageal Manometric Data in Gastroesophageal Reflux Disease, IEEE Transactions on Biomedical Engineering, Vol. 52, no.10, pp.1692-1701, 2005

[32] Z. Lu, J.S. Smith, Q.H.H. Wu, J.E. Fitch, Empirical Mode Decomposition for Power Quality Monitoring, IEEE/PES Transmission and Distribution Conference and Exhibition: Asia and Pacific, 2005

[33] A. Y. Goharrizi, N. Sepehri, Internal Leakage Detection in Hydraulic Actuators Using Empirical Mode Decomposition and Hilbert Spectrum, IEEE Transactions on Instrumentation & Measurement, Vol. 61, no. 2, pp. 368 – 378, 2012

[34] Q. Wu, S.D. Riemenschneider, Boundary Extension and Stop Criteria for Empirical Mode Decomposition, Advances in Adaptive Data Analysis, Vol. 2, no. 2, pp. 157-169, 2010

[35] G. Rilling, P. Flandrin, P. Goncalves, On empirical mode decomposition andits algorithms. IEEE-EURASIP Workshop on Nonlinear Signal and Image Processing NSIP-03, Grado (Italy), 2003

[36] Z. Wu, N.E. Huang, Ensemble Empirical Mode Decomposition: a Noise Assisted Data Analysis Method, Advances in Adaptive Data Analysis, Vol. 1, no. 1, pp.1-41, 2009

[37] M. Zvokelj, S. Zupan, I. Prebil, Multivariate and Multiscale Monitoring of Large-size Low Speed Bearings using Ensemble Empirical Mode Decomposition Method Combined with Principal Component Analysis, Mechanical Systems and Signal Processing, Vol. 24, pp. 1049-1067, 2010

[38] M. Zvokelj, S. Zupan, I. Prebil, Non-Linear Multivariate and Multiscale Monitoring and Signal Denoising Strategy using Kernel Principal Component Analysis Combined with Ensemble Empirical Mode Decomposition Method, Mechanical Systems and Signal Processing, Vol. 25, no. 7, pp. 2631-2653, 2011

[39] J. Zhang, R. Yan, R.X. Gao, Z. Feng, Performance Enhancement of Ensemble Empirical Mode Decomposition, Mechanical Systems and Signal Processing, Vol. 24, pp. 2104-2123, 2010

[40] Q. Gao, C. Duan, H. Fan, Q. Meng, Rotating Machine Fault Diagnosis using Empirical Mode Decomposition, Mechanical Systems and Signal Processing, Vol. 22, pp. 1072-1081, 2008

[41] P. Flandrin, P. Goncalves, G. Rilling, Detrending and Denoising with Empirical Mode Decomposition, XII European Signal Processing Conference (EUSIPCO), September 6-10, Vienna, Austria, 2004

[42] S.J. Loutridis, Damage Detection in Gear Systems using Empirical Mode Decomposition, Engineering Structures, Vol. 26, pp. 1833-1841, 2004

[43] D. Boutana, M. Benidir, B. Barkat, On the Selection of the Intrinsic Mode Function in EMD Method: Application on heart sound signal, 3rd International Symposium on Applied Sciences in Biomedical and Communication Technologies (ISABEL), 2010, Rome, Italy

[44] A. Ayenu-Prah, N.Attoh-Okine, A Criterion for Selecting Relevant Intrinsic Mode Functions in Empirical Mode Decomposition, Advances in Adaptive Data Analysis, Vol. 2, no.1, pp. 1-24, 2010

[45] N. Bu, N. Ueno, O. Fukuda, Monitoring of Respiration and Heartbeat during Sleep using a Flexible Piezoelectric Film Sensor and Empirical Mode Decomposition, Proceedings of the 29th Annual International Conference of the IEEE EMBS, Lyon (France), 2007

[46] J. H. Sullivan, L. A. Jones, A Self-Starting Control for Multivariate Individual Observations, Technometrics, Vol. 44, no. 1, pp. 24-33, 2002

[47] I.T. Jolliffe, Principal Component Analysis, Springer Series in Statistics, 2nd Edition, 2002

[48] P. Stepanic, I.V. Latinovic, Z. Djurovic, A New Approach to Detection of Defects in Rolling Element Bearings based on Statistical Pattern Recognition, International Journal of Advanced Manufacturing Technology, Vol. 45, pp. 91-100, 2009

[49] S. Bersimis, S.Psarakis, J.Panaretos, Multivariate statistical process control charts: an overview, Quality & Reliability Engineering International, Vol. 23, N°5, pp. 517–543, 2006

[50] Z. Zhang, Y. Wang, K. Wang, Intelligent Fault Diagnosis and Prognosis Approach for Rotating Machinery Integrating Wavelet Transform, Principal Component Analysis, and Artificial Neural Networks, International Journal of Advanced Manufacturing Technology, International Journal Advanced Manufacturing Technology, Vol. 68, pp. 763-773, 2013

[51] E. Pinheiro, O. Postolache, P. Girao, Empirical Mode Decomposition and Principal Component Analysis Implementation in Processing Non-Invasive Cardiovascular Signals, Measurements, Vol. 45, pp. 175-181, 2012

[52] T. Lee, T.B.M.J. Ouarda, An EMD and PCA Hybrid Approach for Separating Noise from Signal, and Signal in Climate Change Detection, International Journal of Climatology, Vol. 32, pp. 624-634, 2012

[53] S. Valle, W. Li, S.J. Qin, Selection of the Number of Principal Components: the Variance of Reconstruction Error Criterion with a Comparison to Other Methods, Industrial & Engineering Chemistry Research, Vol. 38, pp. 4389-4401, 1999

[54] S. Wold, Cross-validatory Estimation of the Number of Components in Factor and Principal Components Models, Technometrics, Vol. 20, no. 4, no. 1, pp. 397-405, 1978

[55] P. Nomikos, J.F. MacGregor, Multivariate SPC Charts for Monitoring Batch Processes, Technometrics, Vol 37, no. 1, pp.41-59, 1995

[56] D.C. Montgomery, Introduction to statistical quality control, John Wiley & Sons, Ed. 6, April 2008

[57] M. Goletti, M. Grasso, M. Annoni, B.M. Colosimo, Condition Monitoring of an Ultra High Pressure Intensifier for Waterjet Cutting Machines, Procedia CIRP, Vol. 12, pp. 193-198, 2013

[58] S.L. Sclove, Application of Model-Selection Criteria to Some Problems in Multivariate Analysis, Psychometrika, Vol. 52, no. 3, pp. 333-343, 1987

[59] B. R. Bakshi, Multiscale PCA with Application to Multivariate Statistical Process Monitoring. AIChE Journal, Vol. 4 no. 7, pp. 1596-1610, 1998

[60] Lu N., Wang F., Gao F., Combination Method of Principal Component and Wavelet Analysis for Multivariate Process Monitoring and Fault Diagnosis, Industrial and Engineering Chemistry Research, Vol. 42, pp. 4198-4207, 2003

[61] Zhou S., Sun B., Shi J., An SPC Monitoring System for Cycle-Based Waveform Signals using Haar Transform, IEEE Transactions on Automation Science and Engineering, Vol. 3, no. 1, pp. 60-72, 2006

[62] Coifman, R. R., Wickerhauser, M. V., Entropy-based algorithms for best basis selection, IEEE Transactions on Information Theory, Vol. 38, no. 2, 713-718, 1992